Scale-Invariant Kinematic Comparison of Pressure-Plate Drives in Die-Cutting Presses Using a Unit Nit Displacement Invariant

Vitalii Vlakh
Ph.D.
Independent Researcher
Canada

Ivan Rehei
Dr.Sc, Professor
Institute of Printing and Media Technologies
Lviv Polytechnic National University
Ukraine

Oleh Knysh
Dr.Sc, Professor
Institute of Printing and Media Technologies
Lviv Polytechnic National University
Ukraine

This paper presents an invariant-based framework for scalable kinematic comparison of pressure-plate (platen) drive mechanisms used in die-cutting presses. The maximum platen stroke is adopted as a unit displacement invariant (λS=1), enabling displacement, velocity, and acceleration to be expressed in dimensionless form as functions of the main-shaft angle. Four drive architectures (including wedging- and slider-based layouts) are evaluated using contact-interval metrics defined by a normalized displacement threshold (Si(φ)≥0.98). The proposed approach highlights distinct motion-law features, including asymmetric strokes and long dwell ("plateau") behavior in the contact zone, which is critical for embossing/creasing operations. To validate the analytical invariants, a closed-loop workflow is implemented: mechanism geometry is synthesized in Python, transferred to SolidWorks via automated parameter transfer, and verified using Motion Study results exported to CSV. Experimental acceleration measurements acquired at constant shaft speed further confirm the characteristic shape features of the predicted curves. The presented methodology provides a practical, scale-consistent tool for mechanism selection and motion-law tuning in press applications.

Keywords: similarity theory; dimensionless modelling; invariant normalization; die-cutting press; pressure plate drive; wedging mechanism; kinematic analysis; SolidWorks Motion Study; experimental validation; Python integration.

1. INTRODUCTION

The development of new innovative drives for process equipment remains a key task of modern mechanical engineering. The tightening of requirements for the motion accuracy of the output members, the evolving tool–material interaction requirements, and the need for efficient energy transmission drive the development of new combined lever–wedging systems that meet current process requirements. Such approaches are actively implemented in high-speed manipulators [1], robotic gripping devices [2], and cable-driven flexible/ continuum robotic systems [3]. These trends motivate the need for scale-consistent criteria to compare motion laws of press platen (pressure-plate) drives independently of machine size.

In [4], it is emphasized that modern kinematics is gradually shifting from traditional geometric models to multilevel structures with elements of flexibility and self-adjustment, in which the integration of synthesis, compliance, and tensegrity plays a key role. Such concepts contribute to the development of universal kinematic solutions that can be adapted to different scales or operating conditions without altering the system's basic structure. For press platen drives, this motivates comparison criteria that remain valid when the mechanism is scaled or re-parameterized.

Recent studies increasingly combine kinematics, dynamics, and control to develop formulations that are transferable across mechanism architectures. Analytical motion descriptions for spatial mechanisms enable the generalization of redundant degrees of freedom [5]. At the same time, robotic modeling and experimentally validated compliance-control approaches provide practical tools for representing compliant multibody drives [6]. Advanced nonlinear control of mechanically complex robotic systems further highlights the value of generalized kinematic and dynamic representations for scalable synthesis and comparison [7].

Similarity principles are widely used to transfer results between reduced experiments and full-scale systems, ensuring that scaled testing preserves the underlying physics [8]. Modern treatments systematize geometric, kinematic, and dynamic similarity and emphasize algorithmic procedures for scale transitions in test rigging [9]. Generalized invariance also appears in inertial-parameter identification that links experiments and simulations [10], invariance-preserving control in soft robotics [11], and dimensionless optimal-control formulations for multilink systems [12].

Received: April 2026, Accepted: June 2026
Correspondence to: Vitalii Vlakh, Ph.D.
Independent Researcher
Canada
E-mail: vlakh.v.v@gmail.com
doi: 10.5937/fme2603485V

Motivated by the need for scale-consistent mecha–nism selection, this work introduces invariant kinematic descriptors that enable motion-law comparison inde–pendently of the absolute stroke and speed. The proposed approach adopts the maximum platen (pressure plate) stroke as a unit displacement invariant (λS=1). It represents platen motion using dimensionless displacement, velocity, and acceleration invariants as functions of the main-shaft angle. A contact-zone metric based on a normalized displacement threshold (Si(φ) ≥ 0.98) is used to quantify dwell/plateau behavior and kinematic excitation during die-cutting and creasing. The threshold isolates the near-top region of the stroke where the tool–material interaction is expected to occur.

In die-cutting presses, the platen (pressure plate) motion law strongly affects process quality and machine loading: short, high-acceleration strokes can benefit im–pulse cutting, while creasing/embossing typically requ–ires a controlled dwell (near-constant displacement) in the contact zone. Therefore, the synthesis and com–parison of drive mechanisms should be performed using scalable kinematic criteria that remain valid across machine sizes.

Despite these advances, several limitations remain in the published studies on platen-drive mechanisms. Most studies focus on a single mechanism, report displa–cement, velocity, and acceleration in dimensional units, or optimize only selected structural parameters. As a re–sult, their conclusions are difficult to transfer to presses with different strokes, crank speeds, and geometric scales. In addition, the upper-stroke contact zone is often described qualitatively, whereas mechanism se–lection requires a common metric for evaluating both the duration and smoothness of contact. These short–comings make it difficult to compare different pressure-plate drive architectures on a common basis and to determine whether a mechanism is better suited to impulse die-cutting or creasing/embossing operations.

Therefore, this paper develops a scale-invariant framework for comparing platen displacement, velocity, and acceleration histories. The framework uses the maximum pressure-plate stroke as a unit displacement invariant and introduces a contact-zone metric based on the normalized displacement threshold Si(φ) ≥ 0.98.

The main contributions of this study are as follows:

- a unit-stroke invariant λS=1 is introduced for scale-independent comparison of pressure-plate drives;
- displacement, velocity, and acceleration are repre–sented in a dimensionless form with respect to the main-shaft angle;
- a contact-zone metric based on Si(φ) ≥ 0.98 is used to quantify the duration of the near-top working interval;
- four platen-drive architectures are compared on the same invariant basis; and
- the analytical results are checked through an integ–rated Python–SolidWorks Motion Study–experi–mental workflow.

Classical wedging and eccentric mechanisms of the platen drive have limitations regarding the duration of working contact and the non-uniformity of forces. In [13], a “dual-elbow-bar” mechanism was investigated, and it was shown that the correct choice of the ratio of link lengths and material properties makes it possible to reduce peak loads significantly. In [14], the motion of the die-cutting press platform relative to the crank rotation angle was modeled, which confirmed a signi–ficant dependence of displacement uniformity on the mechanism geometry. Further study [15] substantiated an algorithm-based method for optimizing the drive lever, reducing deformation by 90 percent without loss of stiffness.

Our recent research focuses on modernizing the pla–ten drives of die-cutting presses by introducing addi–tional kinematic contours based on similarity theory. In [16], an analytical model of a wedging mechanism was developed, and the amplitudes of plate oscillations that limit the accuracy of the technological process were determined. In [17], the expediency of a sectional plate structure was substantiated, thereby reducing peak loads. In [18], the dependence of the force parameters of cardboard cutting on the speed characteristics of the drive was experimentally confirmed. In [19], a plate drive using wedging mechanisms was proposed. A pha–se shift between eccentrics is provided to ensure a smooth load distribution. Article [20] presents a compa–rative analysis of various wedging mechanisms in SolidWorks and emphasizes that using an auxiliary crank extends the contact phase between the pressure plate and the material by 12%. In [21], the pressure plate drive model was improved by introducing a gear transmission to create double-wedging contours, thereby doubling the duration of contact between the die tools and the cardboard. Collectively, these results underscore the need for a dimensionless, invariant description that enables direct comparison of motion laws and contact-zone behavior on a common basis.

In this work, the pressure-plate displacement is ado–pted as the unit invariant (λS=1), enabling a dimen–sionless representation in which geometric and kine–matic parameters are normalized by a single criterion, thereby remaining comparable across press sizes.

The framework is implemented in a closed analy–tical–CAD/CAE workflow to verify invariant predic–tions via a parametric SolidWorks Motion Study, with practical relevance to die-cutting/creasing of paperboard blanks where platen-motion stability governs quality [22-24]. Experimental validation of the invariant kine–matic predictions is demonstrated for the two-slider architecture as a representative case, while the rema–ining mechanisms are assessed using the same invariant criteria and CAD/CAE consistency within the work–flow. The remainder of the paper is organized as fol–lows: Section 2 introduces the invariant descriptors and comparison metrics; Section 3 describes the analytical–CAD/CAE–experimental workflow; Section 4 presents and discusses the comparative results.

2. COMPARATIVE ANALYSIS OF MECHANISMS BASED ON SIMILARITY THEORY

2.1 Description of the mechanisms

In the conducted study of the mechanisms, the maxi–mum stroke of the press pressure plate was adopted as λS = 1.0. This makes it possible to derive universal equations of motion and force loading for the press, applicable to both laboratory models and production presses. The main advantage of this methodology is that it provides a scale-independent description of the mechanism's motion. The proposed method enables the creation of generalized analytical models that are independent of the scale parameter. The same equations remain valid for both a prototype with S=20 mm of pressure plate displacement and a production press with S=100 mm or more. Another important advantage is the simplification of geometric synthesis and the prompt optimization of relative geometric parameters (λ1, λ2, λe, etc.) without repeated conversion into absolute dimensions. The mechanism is studied using analytical relationships that remain unchanged under scaling, which accelerates the search for an optimal structure.

The study considers pressure plate drive mecha–nisms in die-cutting presses. In the investigated mecha–nisms: the existing wedging mechanism (Fig. 1a), the two-slider mechanism (Fig. 1b), and the mechanism with an additional driven crank (Fig. 1c), the eccentric mechanisms are placed on the drive shaft. In the double-wedging mechanism (Fig. 1d), gear transmissions are provided to drive the leading cranks of the left and right contours. In all mechanisms, the lower pressure plate 3 is movable. It moves toward the die-cutting form 1, which is fixed to the upper stationary plate 2, by means of the constituent contours 4, 4′. However, the mecha–nisms differ in the structure of the wedging contours, each of which enables specific technological results when processing cardboard blanks during die-cutting.

2.2 Analysis of the kinematic parameters of the investigated mechanisms.

Dimensionless invariants. For each mechanism, the dimensionless displacement invariant is defined relative to the minimum normalized position S_{min}. The dimensionless displacement invariant is defined as:

$$S_i(\varphi) = S(\varphi) - S_{\min} \tag{1}$$

Here $S(\varphi)$ is the dimensionless position of the platen (scaled by the maximum stroke). The quantity S_{min} is the minimum dimensionless position over the cycle. The–refore, $S_i(\varphi)$ is a dimensionless displacement invariant measured from the minimum position and varies within $0 \le S_i \le 1$.

The corresponding dimensionless velocity and acce–leration invariants are defined as derivatives with respect to the crank angle:

$$V_i(\varphi) = \frac{dS_i}{d\varphi}, a_i(\varphi) = \frac{dV_i}{d\varphi} \tag{2}$$

The explicit analytical expressions Si(φ) depend on the mechanism geometry and are derived separately for each investigated structure; in this paper we use those closed-form relations as given in Refs. [20, 21, 25, 26], while Eqs. (1) and (2) provide a common normalization and comparison framework. In this study, all kinematic calculations are performed with the main-shaft angle φ expressed in radians, and the derivatives are taken with respect to radians. For presentation purposes, the plots use φ in degrees on the horizontal axis (i.e., φdeg =180•φ/π), while the invariant velocity and acceleration values remain defined in radians.

Since the displacement of the pressure plate is adopted as the "unit", it is possible to implement a procedure that uses the same normalized graphs of changes in kinematic and force parameters. This makes it possible to directly analyze and compare the parameters of the mechanisms under investigation. The methodology for calculating the kinematic parameters of the investigated mechanisms is presented in the authors' previous studies.

The obtained values of the dependence of the pressure plate displacement on the rotation angle of the main shaft showed its different nature in the plate drive mechanisms: existing wedging (1), two-slider (2), wedging with an additional driven crank (3), and double-wedging (4) (Fig. 2).

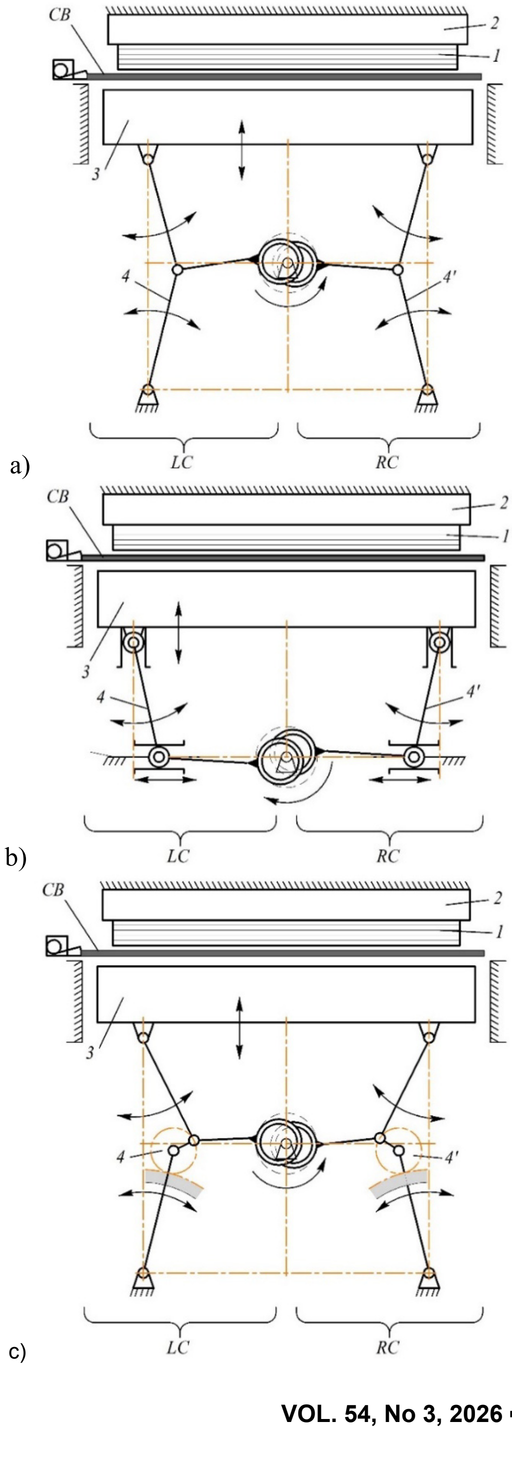

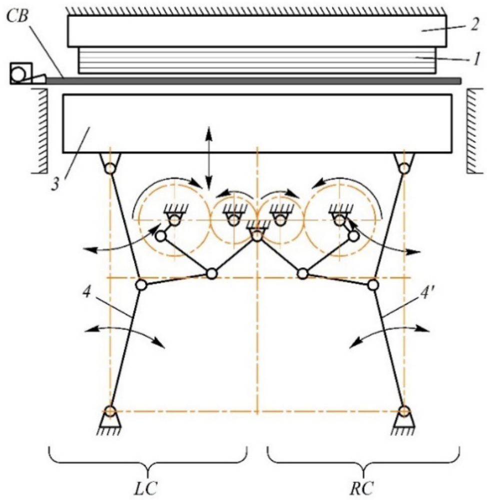

d)

Fig. 1. Kinematic diagrams of the mechanisms: existing wedging (a), two-slider (b), wedging with an additional driven crank (c), double-wedging (d)

A short-term presence of the pressure plate in the die-cutting zone of the cardboard blank is observed under the condition of using wedging mechanisms for its drive (curve 1). The fraction of the duration of contact of the die-cutting tools with the cardboard is 0.07 of the duration of one full revolution of the main shaft. Instead, the use of double-wedging mechanisms in the pressure plate drive significantly extends the duration of die-cutting of blanks (curve 4). In this case, the fraction is 0.32 of the duration of one full revolution of the main shaft, which is a determining condition for ensuring high-quality finishing of cardboard blanks by relief embossing of the material.

The analysis of the graphs showing the dependence of the relative velocity of the pressure plate (PP) on the rotation angle of the main shaft (Fig. 3) showed that the shape of the curves and the peak values depend significantly on the type of kinematic scheme of the drive. For the forward stroke (lifting of the plate), the largest peak values of velocity are observed in the double-wedging (curve 4) and the wedging mechanism with an additional driven crank (curve 3), for which the maximum values are 0.67 and 0.77, respectively. The minimum values during the return stroke reach −1.09 and −0.76; i.e., in the double-wedging mechanism (curve 4), they exceed the positive peak by a factor of 1.62, whereas in the mechanism with the driven crank, they are almost symmetric.

For the existing wedging (curve 1) and the two-slider (curve 2) mechanisms, the maximum values of relative velocity are the same and are about 0.63, while the minimum values are −0.52 and −0.63, respectively. This indicates a short but energetic working cycle: in the two-slider mechanism, the velocity of the forward and return strokes is practically the same, whereas in the wedging mechanism it increases by approximately 1.2 times. Such dynamics are characteristic of the die-cutting process, where a short-term but intensive force of cardboard die-cutting is important.

The analysis of the graphs of the relative acceleration of the pressure plate versus the rotation angle of the main shaft (Fig. 4) confirms significant differences in the mo–tion dynamics in the investigated schemes. At the begin–ning of the cycle (at the angle 0°), the largest initial relative accelerations are observed in the double-wedging mechanism (curve 4) (the values reach 2.017 and 1.319, respectively). This indicates a rapid entry of the plate into the working stroke, but further displacement occurs smo–othly, with an extended segment of uniform motion. For the existing wedging mechanism (curve 1), the initial relative acceleration is only 0.154; for the scheme with the driven crank, it is 0.028; and for the two-slider, it is almost zero. This means that traditional schemes start moving more slowly, whereas improved multilink mechanisms ensure active acceleration from the start of the cycle.

During the forward stroke, the largest peak relative accelerations are recorded in the double-wedging mechanism (curve 4): the maximum relative acceleration is +2.017, and the minimum (during deceleration) is −0.511 (almost 4 times more). Such high values indicate intense acceleration at the beginning of the working phase, but further motion in the die-cutting zone occurs with small accelerations (the motion is practically uniform).

For the mechanism with an additional driven crank, the maximum acceleration in the forward stroke is +0.850, and the minimum is −0.856 (curve 3). In magni–tude, they are almost equal. Such symmetry confirms the balanced operation of the mechanism and a uniform distribution of inertial forces throughout the cycle. The existing wedging mechanism demonstrates moderate changes in relative acceleration (up to +0.386) (curve 1), while the two-slider shows a sharp increase in accele–ration up to −0.590 during the short active die-cutting phase.

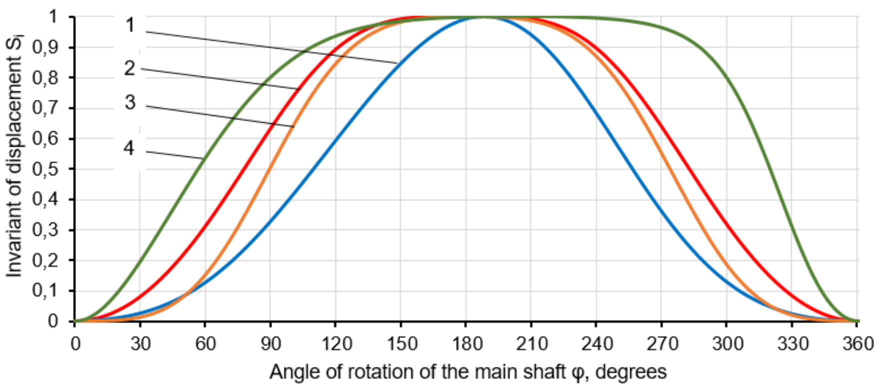

Fig. 2. Plots of the dependence of the relative displacement of the pressure plate on the rotation angle of the main shaft in the mechanisms: existing wedging (1), two-slider (2), wedging with an additional driven crank (3), double-wedging (4)

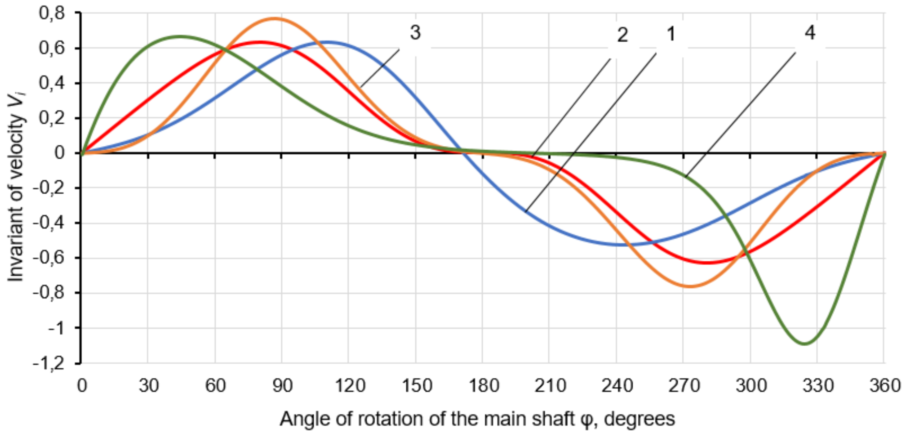

Fig. 3. Plots of the dependence of the relative velocity of the pressure plate on the rotation angle of the main shaft in the mechanisms: existing wedging (1), two-slider (2), wedging with an additional driven crank (3), double-wedging (4)

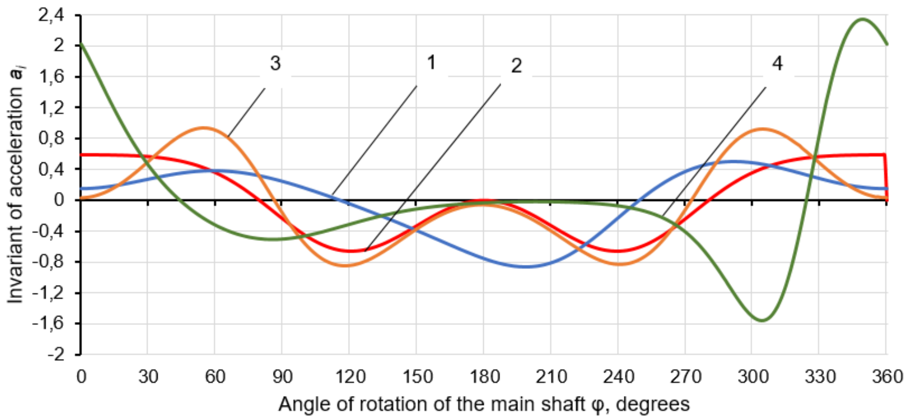

Fig. 4. Plots of the dependence of the relative acceleration of the pressure plate on the rotation angle of the main shaft in the mechanisms: existing wedging (1), two-slider (2), wedging with an additional driven crank (3), double-wedging (4)

During the return stroke, the maximum accele–rations remain high. For the double-wedging mecha–nism, they reach +2.338 (curve 4) and −1.562 (minimum), which indicates a short but dynamic idle stroke. For the mechanism with the driven crank, the maximum relative acceleration during the return stroke reaches +0.924 (curve 3), and the minimum is −0.71, a smooth, balanced motion without sharp jerks. The existing wedging (curve 1) and the two-slider mecha–nisms (curve 2) have symmetric values of ±0.386 and ±0.590, characteristic of simple impulse schemes.

The die-cutting zone of the cardboard blank (Si(φ)≥0.98) is of particular interest. For the double-wedging mechanism (curve 4), it lasts within 146°–259°. In these intervals, the relative acceleration does not exceed values of 0.18–0.33 of the global peaks, which indicates an almost uniform motion of the plate during relief formation. For the mechanism with the driven crank (curve 3), the relative acceleration in the embossing zone is 0.1–0.3, whereas for the existing wedging (curve 1) (176°–200°) and the two-slider (curve 2) (142°–218°) it is significantly higher, and the phase itself is shorter. This indicates an increased inf–luence of inertial forces in traditional schemes, in contrast to the smooth characteristics of the improved mechanisms.

From an operational efficiency standpoint, the double-wedging mechanism (curve 4) offers a rational balance among speed performance, motion smooth–ness, and contact duration in the cardboard embossing zone. Such a mechanism is suitable for both relief embossing of cardboard blanks and combined techno–logical processes. The mechanism with an additional driven crank (curve 3) has the lowest peak loads and is recommended for high-precision presses, where stability and vibration minimization are important. Ins–tead, the existing wedging (curve 1) and the two-slider (curve 2) mechanisms remain expedient for high-speed die-cutting, where a short impulse cycle is an advantage, but the quality of relief forming is limited due to sharp changes in velocity and acceleration.

2.3 Results of the mechanism analysis

In the contact zone, the most pronounced displacement “plateau”, when the pressure plate remains in the contact zone with the cardboard for a relatively long time, is demonstrated by the double-wedging mecha–nism. For this mechanism, the duration of this segment is the greatest (approximately 114° of the cycle angle) (Table 1). Such a shape of the displacement curve during the working stroke means the longest stable contact between the die-cutting tools and the cardboard throughout the cycle, which is directly advantageous for cold embossing and creasing processes: the tools are held longer in working compression without abrupt unloading. The normalized relative velocities and ac–celerations for the upper zone are moderate. The ave–

rage velocity during contact is the lowest among those considered, and the relative acceleration is minimal. Such a design provides a “calm” contact with minimal vibration and better energy indicators of the press. In practice, this means lower peak force loading for the guide structures and joints, better repeatability of the relief (under cold embossing), and reduced wear on parts (which aligns with the motivation for extended contact in the upper phase of the stroke).

The entry and exit angles are obtained by solving $S_i(\varphi)$=0.98, and the duration is $\Delta\varphi=\varphi_{out}-\varphi_{in}$.

Table 1. Contact interval and contact duration for the investigated mechanisms

Mechanism	Contact cycle (°)	$\Delta\varphi$ (°)
Existing wedging	176–200	25
Two-slider	142–218	77
Wedging mechanism with an additional driven crank	150–213	64
Double-wedging	146–259	114

The wedging mechanism, with an additional driven crank, also provides a long contact time between the die-cutting form and the cardboard (during 64° of rotation of the main shaft) and a relatively “calm” average mode. The average relative velocity and acceleration during contact of the die tools with the cardboard are significantly lower than for the “classical” existing wedging and two-slider mechanisms. At the same time, the local peaks of relative velocity here are higher than when using the double-wedging mechanism. This is a compromise, with a long dwell and periodic jumps in relative velocity during entry into and exit from the contact zone. This confirms that adding a driven crank can “stretch” the upper phase and adjust the contact kinematics of an existing wedging mechanism.

The existing wedging mechanisms have a significantly shorter pressure plate displacement in the contact zone with the cardboard. This has a positive effect for “impulse” die-cutting operations (short, energetic cutting of the cardboard), but is worse for embossing/creasing, where a time dwell is required. In the contact zone, the average velocities and especially accelerations in the existing wedging and two-slider mechanisms are the highest among those compared, which is characterized by a more aggressive force mode and increased peak loading on the driving links and guides. Such “stiffness” of kinematics explains the “tendency” of traditional wedge schemes to vibrations and sensitivity to adjustments when overcoming the peak technological resistance of the press.

In the existing wedging mechanism, we observe asymmetric working and idle strokes, and a short dwell of the pressure plate in the zone where the technological die-cutting operation is performed. This leads to an oscillatory motion of the pressure plate, which reduces the operational characteristics of the press compared to the two-slider mechanism. However, the two-slider mechanism possesses ideal symmetry of the working and idle strokes. This is a positive factor that affects the cardboard die-cutting process during short impulse die-cutting. The application of this mechanism improves the operational indicators of the press and ensures higher product quality compared to the existing wedging mechanism in the pressure plate drive.

According to the criterion of the ratio of the working and idle strokes, for all schemes, the working phase ends in the upper part, in which die-cutting, creasing, perforating, and cold embossing of the cardboard occur. For the case when the displacement curve of the pressure plate forms a long horizontal “shelf” (this applies to the double-wedging mechanism, and partly to the wedging mechanism with a driven crank), in the press, during the working stroke, a larger part of the cycle is spent exactly on stable contact. This minimizes instantaneous peaks of velocity/acceleration and “stretches” the load over time. Conversely, in the two-slider and existing wedging mechanisms, the wo–rking phase is shorter and “sharper”: steeper velocity fronts under a narrow angular interval produce a short, jump-like impulse, which imposes additional require–ments on the stiffness of the press structure.

Mechanisms with longer tool contact with the cardboard in the die-cutting zone are characterized by a more uniform working stroke (which contributes to lower vibration loading in the contact zone). However, the idle stroke is shorter and more dynamic, which can cause loading on the supports at the lower position of the pressure plate. In “impulse” schemes, the working stroke is sharp and short, but the idle stroke is distri–buted more uniformly over the cycle without a steep character.

From a practical design perspective, the proposed invariant comparison can be used at the early stage of selecting a platen-drive mechanism for a die-cutting press. Mechanisms with a short contact interval and higher acceleration peaks are better suited to high-speed impulse die-cutting, where a short, energetic working stroke is required. In contrast, mechanisms with an extended contact interval and lower accele–ration in the upper stroke zone are preferable for creasing, embossing, and combined finishing opera–tions, where a more stable contact between the tool and the paperboard blank is needed. Therefore, the pro–posed metric can support the preliminary selection of the drive architecture prior to detailed dynamic analy–sis, prototype manufacturing, or experimental testing.

The influence of platen velocity and acceleration on force characteristics is direct; however, the present study focuses on kinematic similarity. In the adopted dimensionless description, higher acceleration indi–cates stronger inertial excitation for a given reduced mass and transmission ratio. Therefore, mechanisms exhibiting smaller acceleration within the contact interval can be expected to provide a smoother contact regime. A quantitative evaluation of support reactions, driving torque, and damping/clearance requirements requires a coupled force–dynamic model and is left for future work. Such an effect is important for rapid cutting. However, the reverse side is increased force loading and fatigue of the press units. That is why the use of additional links (driven crank) in wedging mechanisms, the addition of an additional wedging contour, or an additional arm to the lower rocker positively influence the functioning of the die-cutting press and improve its technical characteristics.

3. NTEGRATED COMPUTATIONAL-EXPERI–MENTAL VALIDATION FRAMEWORK

If the displacement of the press pressure plate is adopted as unity, then all calculated relationships are formed in a normalized form. During data transfer to SolidWorks, a transformation from invariants to absolute values is performed, which minimizes the risk of errors related to measurement units and facilitates virtual experimen–tation.

To compare the analytical invariant functions with SolidWorks Motion Study and experimental data, the dimensionless invariants are converted to dimensional kinematic quantities using the real maximum pressure plate displacement S_{max} and the shaft angular speed ω:

$$S_r(\varphi) = S_{\max} \cdot S_i(\varphi) \tag{3}$$

$$V_r(\varphi) = \omega \cdot S_{\max} \cdot V_i(\varphi) \tag{4}$$

$$a_r(\varphi) = \omega^2 \cdot S_{\max} \cdot a_i(\varphi) \tag{5}$$

where $\omega=2\pi n/60$ and n is the crankshaft speed in rpm. If needed for consistency checks, SolidWorks/ experimental results in absolute units can be expressed in the invariant form as:

$$\begin{aligned} S_i(\varphi) &= \frac{S_r(\varphi)}{S_{\max}}, \\ V_i(\varphi) &= \frac{V_r(\varphi)}{\omega \cdot S_{\max}}, \\ a_i(\varphi) &= \frac{a_r(\varphi)}{\omega^2 \cdot S_{\max}} \end{aligned} \tag{6}$$

First, the analytical invariants $S_i(\varphi)$, $V_i(\varphi)$, and $a_i(\varphi)$ are computed for a selected mechanism (Fig. 5). Next, the corresponding dimensional geometric parameters are generated and transferred to SolidWorks via the Design Table and Equation Manager. SolidWorks Motion Study is executed to obtain $S_r(t)$, $V_r(t)$, and $a_r(t)$ in absolute units, which are exported to CSV. Finally, the exported results are normalized back to invariant form and used for qualitative shape validation and quantitative comparison of key metrics (contact interval, extrema, and plateau behavior).

Figure 5 provides a schematic overview of the closed-loop workflow used in this study. The pipeline starts from analytical invariant functions, generates a dimensional mechanism model, and transfers parameters to SolidWorks via COM automation. After executing the Motion Study, the kinematic outputs are exported and used to validate the analytical invariant predictions (locations of extrema, plateau behavior, and contact-interval metrics).

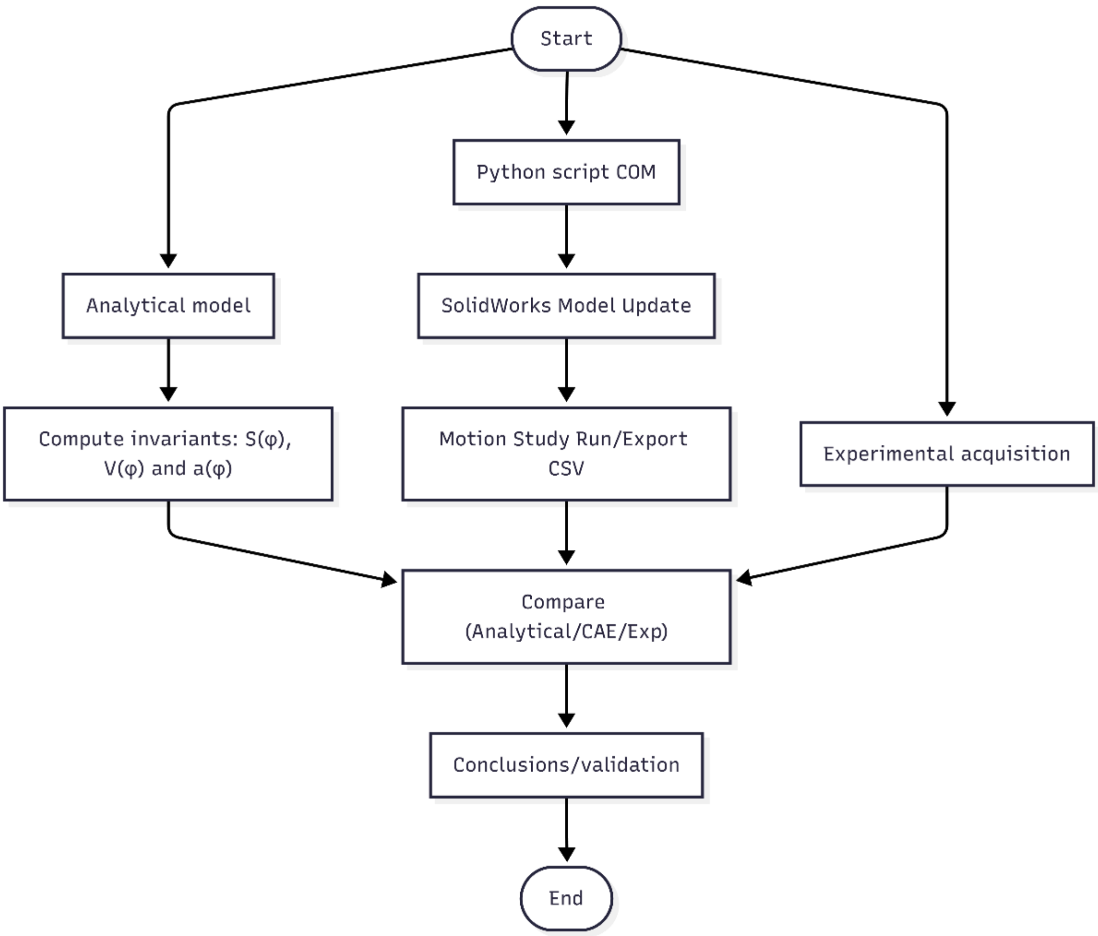

Fig. 5. Workflow of the automated SolidWorks Motion Study, data export, and validation against analytical invariants and experimental result

3.1 Python-Based Kinematic Modeling and Data Integration

The Python routine synthesizes the dimensional geo–metry from the selected invariant parameters, writes the values to the SolidWorks Design Table/Equation Mana–ger, executes a Motion Study, and exports Sr(t), Vr(t), and ar(t) for subsequent comparison with analytical invariants and experimental records.

This creates a closed analysis loop: analytical calcu–lations for invariants, then Python provides synthesis and normalization of parameters, SolidWorks performs a virtual experiment, and the results in the form of displacement, velocity, and load graphs are exported into a table for comparison with analytical invariants. This not only confirms the correctness of the calcula–tions, but also enables efficient parametric optimization of designs by varying relative coefficients and imme–diately observing their influence on the mechanism behavior.

This approach directly links similarity-based analy–tical calculations with numerical modelling and experi–mental verification. It makes the design process faster and reduces the risk of errors during the transition from invariant parameters to dimensional CAD/CAE models.

3.2 SolidWorks CAD/CAE Simulation Workflow

The layout of the experimental rig for the two-slider mechanism is shown in Fig. 6. The configuration repro–duces the actual motion of the two-slider mechanism used in a die-cutting press, with full preservation of the geometric relationships among links and joints. The main linear dimensions of the mechanism, including the link lengths L_1 and L_2, the length of the driving crank L_R, and the overall dimensions H and W, were obtained by designing the rig and transferred to SolidWorks. These parameters determine the working stroke of the plate S and serve as the basis for constructing an accurate 3D model in SolidWorks.

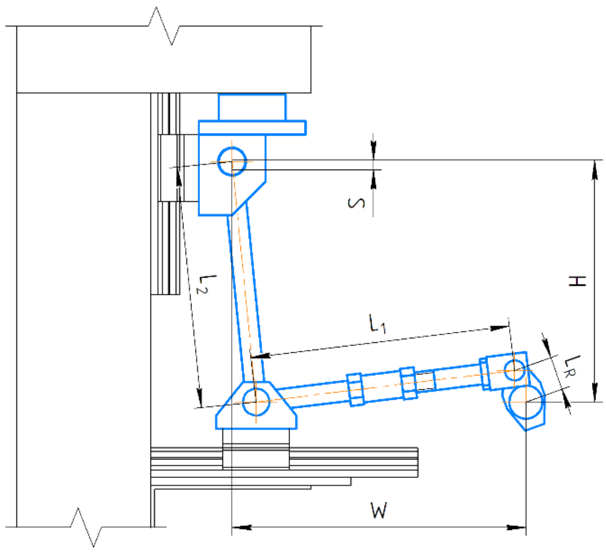

Fig. 6. Schematic diagram of the experimental rig for studying cardboard die-cutting

Table 2 presents all the main dimensions used for CAD reconstruction. Exact correspondence between physical measurements and CAD parameters is critical for achieving realistic mechanism behavior when mo–deling in SolidWorks Motion Study. This ensures correct kinematic trajectories, accurate interaction of elements, and reliable subsequent verification in the experiment.

Based on the generalized parameters, a complete 3D model of the experimental rig was built in SolidWorks (Fig. 7: 1 - driving crank; 2, 3 - connecting rods, 4 - pressure plate). Each element of the mechanism (links, support blocks, guides, and load-bearing frame) was modeled as a separate part and assembled using approp–riate mates corresponding to real kinematic pairs. The created model enables dynamic analysis in Motion Study to simulate the displacement, velocity, and acce–leration of the pressure plate. The obtained simulation results are further compared with the physical experi–ment data to assess the accuracy of the analytical model.

Table 2. Main geometric parameters of the test rig

Parameter	Value, in	Value, mm
W	8.661	220
H	7.087	180
L_R	0.985	25
L_1	7.678	195
L_2	7.087	180
S	0.279	7.084

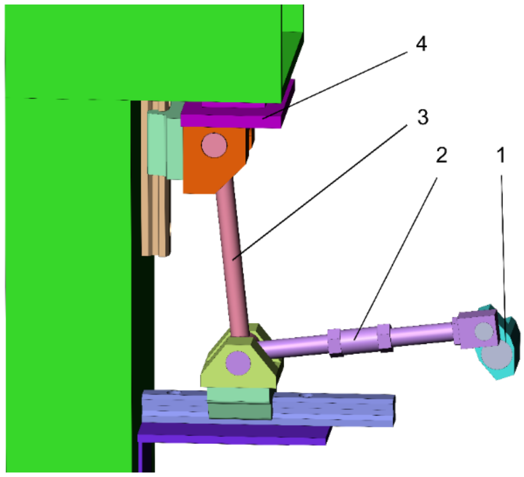

Fig. 7. 3D model of the experimental rig with a two-slider drive mechanism of the pressure plate

3.3 Experimental Setup and Measurement Procedure

To verify the analytical calculations and to compare them with the CAD/CAE analysis based on similarity theory, a test rig (Fig. 8: 1 - driving crank; 2, 3 - connecting rods, 4 - pressure plate) of a flat-bed die-cutting press with a combined (double-crank–slider) drive of the lower pressure plate was manufactured. The drive was implemented from a P31M DC motor (1.4 kW, $n \approx 1500$ rpm) through a two-stage V-belt trans–mission ($u_1=5.6$; $u_2=2.3$; $u_\Sigma \approx 12.8$), which provides the operating range of the drive-shaft rotational speed and the possibility to regulate the speed of the cardboard die-cutting process. The crank–slider contours were implemented on profiled ball guides. In the driven contour, the lower pressure plate with the tool (cutting rule, ejector elements) is fixed. The following were used for measurements: a strain-resistive module on the shaft (bridge circuit with temperature compensation), a non-contact laser tachometer DT-2234C for monitoring n, and an accelerometer (MMA7361 + ATmega8a + Bluetooth HC-05) for acceleration.

The experiments were performed at a fixed crank rotational speed of n = 160 rpm with synchronous measurement of the pressure plate acceleration. Signal processing was carried out in MS Excel.

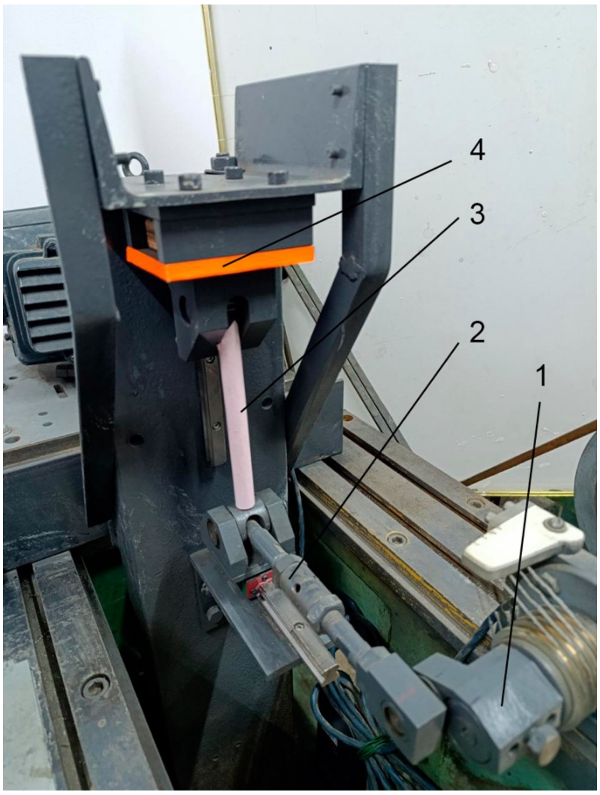

Fig. 8. Photo of the test rig

3.4 Comparative Evaluation of Simulation and Experimental Results

The results of experimental studies of the pressure plate acceleration in the form of a graph are shown in Fig. 9. The X-axis represents time, which is equal to dividing the number of obtained experimental values by the sampling frequency of the analog-to-frequency con–verter. The accelerometer sampling rate was $f_s=1/\Delta t \approx 333$ Hz (Δt=0.003 s); therefore, $t=k/f_s$, where k is the sample index. The study presents the results at a drive shaft rotational speed of 160 rpm. The experimental and SolidWorks results are presented in the time domain (Fig. 9), while the analytical invariant form is presented versus shaft angle for mechanism comparison (Fig. 10).

As can be seen from the experimental diagram (1) in Fig. 9, the instantaneous values of the plate acceleration exhibit characteristic non-uniformity, manifested as high-frequency oscillations around the main trajectory. Such fluctuations are typical for real mechanical systems and are caused by the presence of clearances in kinematic pairs, micro-irregularities of contact surfaces, fluctuations of the drive torque, and noises of analog-to-digital conversion. Despite these features, the overall shape of the experimental curve clearly reproduces the mechanism's main kinematic cycle and agrees with the theoretically predicted dynamics.

The simulation in SolidWorks Motion Study (curve 2 in Fig. 9) demonstrates a smoothed, but structurally similar characteristic of the acceleration variation during a full shaft revolution. The amplitudes and phases of the extreme points in the model coincide with the experimental values. Minor deviations observed at the beginning and in the zone of accelerated motion are associated with the mathematical idealization of the CAD model, where real elastic deformations, micro-displacements in joints, and drive torque fluctuations are absent. Thus, SolidWorks provides a correct reproduction of the real dynamics of the mechanism and confirms the accuracy of the developed 3D kinematics.

The analytical model describes the plate displacement invariants as a function of the main shaft's rotation angle and demonstrates a combined character of the acceleration variation. The input parameters for calculating the invariants of displacement, velocity, and acceleration of the pressure plate are:

W - horizontal distance between the supports of the two-slider mechanism;

λ_r - crank radius;

λ_1, λ_2 - length of the horizontal and vertical connecting rods;

The displacement invariant of the pressure plate is determined by the relationship:

$$S_i(\varphi) = \sqrt{\lambda_2^2 - X_1 - S_{\min}} \tag{7}$$

where

$$X_1 = \left(\sqrt{\lambda_1^2 - \lambda_r^2 \cdot \sin(\varphi)} - \lambda_r \cdot \cos(\varphi)\right)^2 \tag{8}$$

The velocity invariant of the pressure plate:

$$V_i(\varphi) = \frac{A \cdot \lambda_r \cdot X_2}{\sqrt{\lambda_2^2 - A^2}} \tag{9}$$

where

$$\begin{aligned} X_2 &= \sin(\varphi) \cdot \left(1 - \frac{\lambda_r \cdot \cos(\varphi)}{\sqrt{\lambda_2^2 - \lambda_r^4 \cdot \sin(\varphi)^2}}\right), \\ A &= W - \left(X_3 - \lambda_r \cdot \cos(\varphi)\right), \\ X_3 &= \sqrt{\lambda_1^2 - \left(\lambda_r \cdot \sin(\varphi)\right)^2} \end{aligned} \tag{10}$$

The acceleration invariant of the pressure plate:

$$a_i(\varphi) = \frac{\lambda_2^2 \cdot B \cdot C}{\left(\lambda_2^2 - A^2\right)^{3/2}} + \frac{A \cdot D}{\sqrt{\lambda_2^2 - A^2}} \tag{11}$$

where

$$B = \lambda_r \cdot \sin(\varphi) \cdot \left(\frac{\lambda_r \cdot \cos(\varphi)}{\sqrt{\lambda_1^2 - \lambda_r^4 \cdot \sin(\varphi)^2}} - 1\right) \tag{12}$$

$$C=\lambda_r\cdot\sin(\varphi)-\left(1-\frac{\lambda_r\cdot\cos(\varphi)}{\sqrt{\lambda_1^2-\lambda_r^4\cdot\sin(\varphi)^2}}\right) \tag{13}$$

$$D=\lambda_r\cdot\cos(\varphi)-\frac{\lambda_r^2}{\sqrt{\lambda_1^2-\lambda_r^4\cdot\sin(\varphi)^2}}\cdot$$
$$\cdot\left(\left(\cos(\varphi)^2-\sin(\varphi)^2\right)+X_i\right), \tag{14}$$
$$X_4=\frac{\lambda_r^2\cdot\left(\cos(\varphi)^2-\sin(\varphi)^2\right)}{\lambda_1^2-\lambda_r^4\cdot\sin(\varphi)^2}$$

Figure 10 presents the analytical dimensionless acceleration invariant as a function of the main-shaft rotation angle. Figure 9, in contrast, shows the measured and simulated (SolidWorks) dimensional acceleration as a function of time. Since the experiment is conducted at a constant shaft speed, the time and angle parame–terizations are linearly related; therefore, Fig. 10 is used for qualitative visual validation of the cycle shape (lo–cations of extrema and overall trend), rather than for point-by-point numerical matching with Fig. 9.

The high correlation between theoretical and prac–tical results indicates that the model can be used not only to analyze existing mechanisms but also to predict the behavior of new design solutions. In particular, the correctness of the analytical description enables optim–ization of the mechanism's geometric parameters, modeling the effects of changes in link lengths or joint location angles, and evaluating drive loads under different operating modes without the need to conduct a significant number of costly experiments.

4. CONCLUSIONS

In the article, the displacement S of the pressure plate of a die-cutting press is adopted as the basic invariant (λ_S=1), which normalizes the relative geometry, velocity, and acceleration of the plate. In such a dimensionless description, the shape of the kinematic functions is determined only by the relative parameters of the mechanism structure, and not by the scale of the model. A comparison of the experimental and analytical graphs of the relative acceleration of the pressure plate showed a coincidence of the characteristic features of the curves (extrema, plateaus in the contact zone, zero acceleration at the moment of die-cutting) during the transition from the laboratory rig to the production design of the press. As a result, the invariant relationships are correctly “transferred” in the scale category. This is the practical validation of similarity: the same dimensionless model explains the behavior of both the prototype and the real machine.

The proposed unit-displacement normalization pro–vides a practical tool for early-stage selection and tuning of platen-drive mechanisms. It allows mechanisms with different absolute strokes and dimensions to be compared using the same displacement, velocity, acceleration, and contact-zone metrics. This is useful when selecting a drive layout for a specific technological process: short, more dynamic contact intervals can be acceptable for high-speed impulse die-cutting, whereas longer, smoother contact intervals are preferable for creasing and embossing.

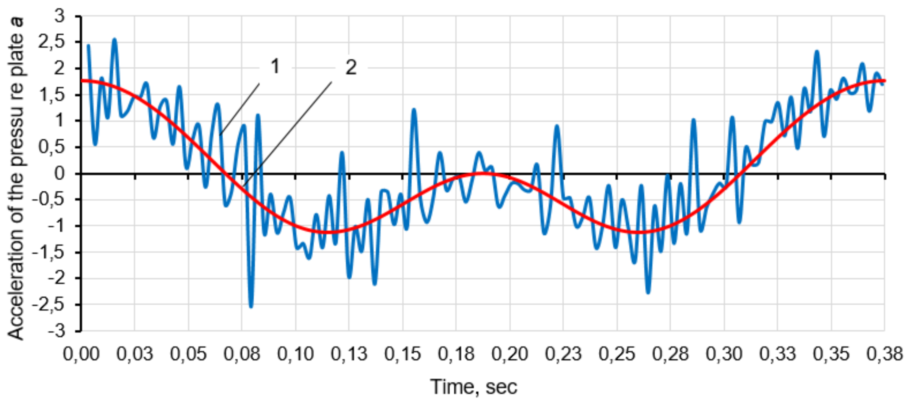

Fig. 9. Experimental acceleration of the pressure plate (curve 1) and SolidWorks Motion Study result (curve 2) at *n=160 rpm*.

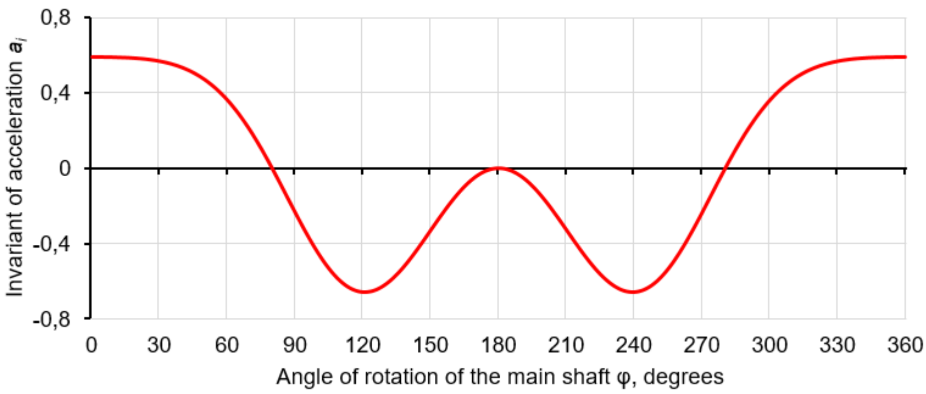

Fig. 10. Analytical dimensionless acceleration invariant of the pressure plate versus the main-shaft angle for the two-slider drive (used for qualitative shape validation of the cycle).

The method also reduces the dependence on repeated dimensional recalculation during CAD/CAE modeling. Once the relative parameters are selected, the same invariant curves can be converted into dimen–sional values for a particular press size and shaft speed. Therefore, the approach can support preliminary mec–hanism selection, parameter tuning, SolidWorks Motion Study preparation, and comparison with experimental measurements.

Limitations and future work. The present experi–mental validation is conducted for the two-slider mec–hanism due to the available test rig configuration. Ex–tending the same measurement protocol to the other drive architectures and adding a coupled force–dynamic model to estimate support reactions and drive torque will be addressed in future work.

REFERENCES

[1] Liu, Y., and Ben-Tzvi, P., 2021, "A New Extensible Continuum Manipulator Using Flexible Parallel Mechanism and Rigid Motion Transmission," Journal of Mechanisms and Robotics, 13(3), p. 031014, https://doi.org/10.1115/1.4050097

[2] Ngo, H. Q. T., et al., 2024, "Investigation on the Mechanical Design of Robot Gripper for Intelligent Control using the Low-cost Sensor," FME Transactions, 52(1), pp. 12–28.

[3] Amouri, A., and Rahma, O., 2026, "Design, Modeling, and Validation of a Self-Balancing Cable-Driven Continuum Robot Using Internal Force Equilibrium," FME Transactions, 54(1)

[4] McCarthy, J. M., 2011, "21st Century Kinematics: Synthesis, Compliance, and Tensegrity," Journal of Mechanisms and Robotics, 3(2), p. 020201, https://doi.org/10.1115/1.4003181

[5] Garriga-Casanovas, A., and Rodriguez y Baena, F., 2019, "Kinematics of Continuum Robots With Constant Curvature Bending and Extension Capabilities," Journal of Mechanisms and Robotics, 11(1), p. 011010, https://doi.org/10.1115/1.4041739

[6] Petrović, P. B., Danilov, I. R., et al., 2017, "Configuration-based Compliance Control of Kinematically Redundant Robot Arm – Part II: Experimental Validation," FME Transactions, 45(4).

[7] Amouri, A., Cherfia, A., Merabti, H., and Laib Dit Leksir, Y., 2022, "Nonlinear Model Predictive Control of a Class of Continuum Robots Using Kinematic and Dynamic Models," FME Transactions, 50(2), pp. 339–350.

[8] Podeur, M., and Vogt, D. M., 2022, "Experimental and Numerical Similitude Study Using a Novel Turbocompressor Test Facility Operating With Helium–Neon Gas Mixtures," Journal of Turbomachinery, 144(8), p. 081015, https://doi.org/10.1115/1.4053987

[9] Casaburo, A., Petrone, G., Franco, F., and De Rosa, S., 2019, "A Review of Similitude Methods for Structural Engineering," Applied Mechanics Reviews, 71(3), p. 030802, https://doi.org/10.1115/1.4043787

[10] Gautier, M., and Khalil, W., 1990, "Direct Determination of Minimum Inertial Parameters of Robots," IEEE Transactions on Robotics and Automation, 6(3), pp. 368–373.

[11] Liu, D., et al., 2023, "Residual Reinforcement Learning Based on Inverse Kinematic Modeling for Soft Robotic Arm Control," IEEE/ASME Transactions on Mechatronics, 28(4), pp. 1802–1813, https://doi.org/10.1109/TMECH.2023.3241570

[12] Eichmeir, P., Lauß, T., Oberpeilsteiner, S., Nachbagauer, K., and Steiner, W., 2021, "The Adjoint Method for Time-Optimal Control Problems," Journal of Computational and Nonlinear Dynamics, 16(2), p. 021003, https://doi.org/10.1115/1.4048808

[13] Lin, W. G., Zhou, C., and Huang, W. J., 2015, "Optimum Design for Mechanical Structures and Material Properties of the Dual-Elbow-Bar Mechanism," Advances in Materials Science and Engineering, 2015, Article ID 724171, https://doi.org/10.1155/2015/724171

[14] Zhou, Y., Cheng, B., Yang, H., and Wang, C., 2024, "Simulation of the Relationship Between Die-Cutting Moving Platform and Crankshaft Motion," Frontiers in Artificial Intelligence and Applications, 382, pp. 148–153, https://doi.org/10.3233/FAIA231293

[15] Wang, J., Chen, X., and Li, Y., 2023, "Structure Design and Optimization Algorithm of a Lightweight Drive Rod for Precision Die-Cutting Machine," Applied Sciences, 13, p. 4211, https://doi.org/10.3390/app13074211

[16] Vlakh, V. V., and Mykhailiv, Yu. Yu., 2023, "Research on the Pressure Plate Movement by the Drive With Wedging Mechanisms in the Die-Cutting Press," Printing and Publishing, 2(86), pp. 174–184, https://doi.org/10.32403/0554-4866-2023-2-86-174-184

[17] Rehei, I., Vlakh, V., and Mykhailiv, Y., 2023, "Technical Justification of the Sectional Construction of the Pressure Plate in the Die-Cutting Press," Proceedings of the International Scientific Discussion Conference, https://doi.org/10.51582/interconf.19-20.03.2023.055

[18] Knysh, O., Rehei, I., Vlakh, V., Mlynko, O., and Ternytskyi, S., 2023, "Analytical Interpretation of Experimental Research of Cardboard Cutting in Die-Cutting Press," Academic Journal of Manufacturing Engineering, 21(1), pp. 43–49.

[19] Rehei, I., Knysh, O., Vlakh, V., and Mykhailiv, Y., 2023, "Sectional Design of the Pressure Plate in the Die-Cutting Press With Wedging Mechanisms: Justification of Application," Proceedings of the 1st International Scientific and Practical Conference "Modern Knowledge", https://doi.org/10.51582/interconf.19-20.05.2023.031

[20] Vlakh, V. V., 2023, "Comparative Analysis of the Kinematic Parameters of the Wedging Drive Mechanisms of the Die-Cutting Presses Using the SolidWorks Software," Printing and Publishing,

1(85), pp. 174–183, https://doi.org/10.32403/0554-4866-2023-1-85-174-183

[21] Vlakh, V. V., Rehei, I. I., and Knysh, O. B., 2025, "Research of the Wedging Mechanism With Additional Driven Crank and Gear Transmission in the Pressure Plate Drive of the Die-Cutting Press," Australian Journal of Mechanical Engineering, https://doi.org/10.1080/14484846.2025.2459456

[22] Hünniger, J., Engisch, L., Hamblyn, S., Käppeler, U., and Hofmann, A., 2022, "Influence of Ultrasound on Embossing Results for Cardboard," BioResources, 17(4), pp. 5803–5819, https://doi.org/10.15376/biores.17.4.5803-5819

[23] Käppeler, U., Hünniger, J., Hofmann, A., Berlich, A., and Engisch, L., 2020, "Thermal Influence on the Mechanical Properties of Cardboard During an Ultrasonic-Assisted Embossing Process," BioResources, 15(3), pp. 5110–5121, https://doi.org/10.15376/biores.15.3.5110-5121

[24] Käppeler, U., Schneller, K., Wallburg, F., Engisch, L., and Schoenfelder, S., 2022, "Analysis of the Compression Behavior of Different Cardboard Materials During Embossing," Open Conference Proceedings, 2, p. 132, https://doi.org/10.52825/ocp.v2i.132

[25] Rehei, I., Vlakh, V., Knysh, O., and Mlynko, O., 2023, "Combined Double Crank Wedging Drive Mechanisms of the Press Plate Used in Die-Cutting Press: Synthesis, Kinematic and Functional," Academic Journal of Manufacturing Engineering, 21(3), pp. 53–60.

[26] Vlakh, V., Rehei, I., and Knysh, O., 2025, "Geometric Synthesis and Kinematic Analysis of a Combined Double-Wedging Mechanism of the Pressure Plate Drive in the Die-Cutting Press," Journal of Graphic Engineering and Design, 16(4), pp. 13–24, https://doi.org/10.24867/JGED-2025-4-013

NOMENCLATURE

λ_S	normalized maximum stroke (base invariant), λS = 1.0
φ	crankshaft rotation angle, rad
$S_i(\varphi)$	invariant (dimensionless) displacement of the pressure plate as a function of φ
S_{min}	dimensionless minimum (reference) value used in the invariant displacement definition
$V_i(\varphi)$	invariant (dimensionless) velocity of the pressure plate as a function of φ
$a_i(\varphi)$	invariant (dimensionless) acceleration of the pressure plate as a function of φ
$S_r(\varphi)$	displacement of the pressure plate as a function of φ, mm
$V_r(\varphi)$	velocity of the pressure plate as a function of φ, mm/s
$a_r(\varphi)$	acceleration of the pressure plate as a function of φ, mm/s2
$S_r(t)$	displacement of the pressure plate as a function of t, mm
$V_r(t)$	velocity of the pressure plate as a function of t, mm/s
$a_r(t)$	acceleration of the pressure plate as a function of t, mm/s2
ω	crankshaft speed, rad/s
S_{max}	maximum platen (pressure plate) displacement, mm
W	horizontal distance between the supports of the mechanism (used for the test rig and in the analytical model), mm
H	overall height (characteristic vertical dimension) of the test rig, mm
L_R	driving crank length (or crank radius parameter for the rig), mm
L_1, L_2	link lengths (connecting rods) of the experimental rig, mm
λ_r	crank radius (relative/invariant parameter in the analytical model)
λ_1, λ_2	lengths of the horizontal and vertical connecting rods (relative/invariant parameters in the analytical model)
A, B, C, D	auxiliary expressions introduced for compact representation of the invariant velocity and acceleration equations (dimensionless)
n	rotational speed of the crank, rpm

ACRONYMS AND ABBREVIATIONS

CSV	Comma-Separated Values
CAD	Computer-Aided Design
CAE	Computer-Aided Engineering
DC	Direct Current
COM	Component Object Model
PP	Pressure Plate
rpm	revolutions per minute

КИНЕМАТСКО ПОРЕЂЕЊЕ ПОГОНА ПРИТИСКА ПЛОЧЕ У ПРЕСАМА ЗА СЕЧЕЊЕ, ИНВАРИЈАНТНО У ОДНОСУ НА СКАЛУ, КОРИШЋЕЊЕМ ЈЕДИНИЧНЕ ИНВАРИЈАНТЕ ПОМЕРАЊА

В. Влах, И. Рехеј, О. Книш

Овај рад представља оквир заснован на инваријанти за скалабилно кинематско поређење механизама погона притиска плоче (плоче) који се користе у пресама за сечење. Максимални ход плоче је усвојен као јединична инваријанта померања (λS=1), што омогућава изражавање померања, брзине и убрзања у бездимензионалном облику као функције угла главног вратила. Четири архитектуре погона (укључујући распореде засноване на клинању и клизању) су процењене коришћењем метрика контактног интервала дефинисаних нормализованим прагом померања (Si(φ)≥0,98). Предложени приступ истиче различите карактеристике закона кретања, укључујући асиметричне потезе и понашање дугог задржавања („плато“) у зони контакта, што је критично за операције утискивања/савијања. Да би се валидирале аналитичке инваријанте, имплементиран је ток рада затворене петље: геометрија механизма је синтетизована у Пајтону, пренета у SolidWorks

путем аутоматизованог преноса параметара и верификована коришћењем резултата студије кретања извезених у CSV. Експериментална мерења убрзања добијена при константној брзини вратила додатно потврђују карактеристичне особине облика предвиђених кривих. Представљена методологија пружа практичан, скала-конзистентан алат за избор механизма и подешавање закона кретања у применама преса.